Overlayer-induced ordering of the disordered surface monolayer in Langmuir-Blodgett multilayer thin films

V. Skita, W. Richardson, M. Filipkowski, A. Garito, J.K. Blasie

J. Physique **47** (1986) 1849-1855 OCTOBRE **1986**, PAGE 1849

Classification
Physics Abstracts
68.55

Overlayer-induced ordering of the disordered surface monolayer in Langmuir-Blodgett multilayer thin films

V. Skita ([a]), W. Richardson ([b]), M. Filipkowski ([c]), A. Garito ([c,d]) and J. K. Blasie ([a,b,d])

Departments of Biochemistry-Biophysics ([a]), Chemistry ([b]), Physics ([c]), and the Laboratory for Research on the Structure of Matter ([d]), University of Pennsylvania, Philadelphia, Pennsylvania 19104, U.S.A.

(*Reçu le 14 novembre 1985, révisé le 5 juin 1986, accepté le 5 juin 1986*)

Résumé. — On présente une expérience de diffusion des rayons X par des films de Langmuir-Blodgett. Les résultats montrent que la monocouche de surface à l'interface film multicouches/air est désordonnée, et qu'elle peut être réordonnée par dépôt d'une monocouche supplémentaire. Les données sont analysées au moyen d'une nouvelle technique qui calcule la fonction d'autocorrélation du profil du film sans supposer la structure centrosymétrique et sans postuler l'existence d'une cellule unité.

Abstract. — X-ray scattering results from Langmuir-Blodgett thin films demonstrate that the surface monolayer at the multilayer-air interface is disordered and that ordering of the surface monolayer can be induced by the deposition of an additional monolayer. The data was analysed by a novel refinement technique which does not assume a centrosymmetric structure or the existence of a unit cell.

1. Introduction.

Multilayer thin films can be fabricated by the Langmuir-Blodgett technique to produce finite sequences of from one to several hundred molecular monolayers of different amphiphilic molecules [1]. Both periodic and quasi-periodic sequences can be constructed using two, or more, molecules of different incommensurate chain lengths. If one of the molecules contains a π-electron system possessing a large nonlinear optical response, the macroscopic nonlinear optical properties of such thin films can be controlled [2]. This depends critically on the nature of the structural ordering of the molecular sites along the profile axis of the multilayer perpendicular to the layer planes as well as in the plane of the monolayers. Most methods of unambiguous structural analysis employing X-ray scattering require the repetition of some average structural unit (unit cell) in a periodic array of effectively infinite extent. We have previously employed novel methods in the analysis of the X-ray scattering perpendicular to the layer planes from finite periodic multilayer films containing from two to ten molecular monolayers [3]. This communication reports on the extension of these methods to finite, quasiperiodic multilayer structures. They have been utilized to prove that the surface monolayer at the multilayer-air interface is disordered in such thin films and that ordering of the surface monolayer occurs on subsequent deposition of an additional bilayer.

2. Methods

Two sets of multilayers were used for this study. They were 1) finite sequences of arachidic acid (A) $\left[CH_3-\left(CH_2\right)_{18}-COOH\right]$ and myristic acid (M) $\left[CH_3\left(CH_2\right)_{12}-COOH\right]$ monolayers and 2) finite sequences of arachidic acid and 10, 12 pentacosadiynoic acid

$$\left[CH_3-\left(CH_2\right)_{11}-C\equiv C-C\equiv C-\left(CH_2\right)_8-COOH\right]$$

monolayers. The 10, 12 pentacosadiynoic acid monolayers were polymerized with uv light to form diacetylene polymer (D) (the polyene polymer chains being perpendicular to the monomer hydrocarbon chains).

Specimens were prepared by depositing the macromolecular monolayers by the Langmuir-Blodgett (LB) technique on a flat glass substrate which was made hydrophobic by covalently binding an octadecyltrichlorosilane (OTS) monolayer to its surface [4].

The fatty acid monolayers were deposited at a temperature of 17.5 °C at a constant surface pressure of 15 dyne/cm for the myristic acid and 20 dyne/cm for the arachidic acid and the 10, 12 pentacosadiynoic acid ; the subphase was a 1mM $CdCl_2$ solution of pH < 6.0. The LB trough system, monolayer film properties, and details of the deposition conditions are described elsewhere [3].

Meridional X-ray diffraction was obtained from the multilayers as a function of

$$q_z \left[q_z \equiv (2 \sin \theta)/\lambda \right]$$

corresponding to elastic photon momentum transfers parallel to the z-axis perpendicular to the substrate plane. This meridional X-ray diffraction arises from the projection of the three dimensional multilayer electron density distribution along radial vectors lying in the layer planes perpendicular to the z-axis onto the z-axis ; the projection is defined as the electron density profile for the multilayer. The incident X-ray beam defines an angle omega (ω) with the substrate plane (x-y). Meridional X-ray diffraction is observed for ω equal θ, where 2 θ is the angle between the incident and scattered beams. The multilayers were therefore positioned on the ω axis of a two-axis Hüber diffractometer which was scanned over an appropriate range of values permitting the collection of the meridional diffraction data with a low impedance position-sensitive detector (PSD) aligned along the q_z direction and mounted on the 2 θ axis. An Elliott (GX-6) rotating anode X-ray generator was used to produce the incident Cu K X-rays at a target loading of ~ 2.5 KW /mm^2. K_α X-rays were selected with a nickel filter and focused at the PSD entrance window *via* Franks optics.

Details regarding multilayer sample conditions and omega scan parameters have been outlined in our previous paper [3]. Each omega scan took approximately 10 hours, resulting in a composite pattern which represents the meridional intensity function $I(q_z)$. The intensity functions were corrected for background scattering followed by a Lorentz correction of q_z to correct for oscillation of the multilayers in the ω-scan to yield the corrected intensity function $I_0(q_z)$.

3. Results.

Figure 1 shows the corrected intensity functions for the first set of multilayer films. These multilayers consist of two arachidic acid monolayers deposited onto the glass-OTS substrate followed by the deposition of either a) two arachidic acid monolayers to yield two arachidic acid bilayers (AAAA), b) one arachidic acid monolayer followed by a myristic acid monolayer to yield three arachidic acid monolayers and one myristic acid monolayer (AAAM), or c) two myristic acid monolayers to yield an arachidic acid bilayer followed by a myristic acid bilayer (AAMM).

All the corrected intensity functions in figure 1 are

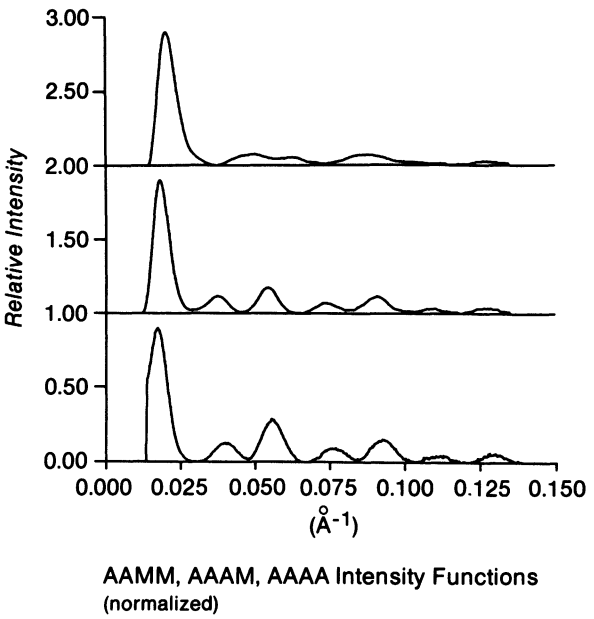

Fig. 1. — The background and Lorentz-q_z corrected intensity functions for the AAMM (top), AAAM (middle), and AAAA (bottom) multilayers are shown. Due to the relatively low signal to noise ratio of the AAMM and AAAM intensity functions when compared to the AAAA intensity function, the AAMM and AAAM intensity functions were smoothed.

indicative of asymmetric multilayer profiles of finite size or extent. The non-zero minima between diffraction maxima indicate that the profiles are asymmetric while the broad shape of the maxima results from their finite extent [3]. The meridional X-ray diffraction from multilayers composed of periodic sequences of monolayers should contain the most pronounced constructive and destructive interference effects. Such interference effects should be diminished in the diffraction from multilayers composed of non-periodic sequences of monolayers. The AAAA multilayer to first approximation is periodic composed of two arachidic acid bilayers ; diffraction from the multilayer consequently contains stronger interference effects than the AAAM and AAMM multilayers. The AAAM multilayer corrected intensity function is similar to the AAAA multilayer corrected intensity function except for the somewhat lesser relative magnitudes of the diffraction maxima at higher q_z. The corrected intensity function for the AAMM multilayer differs considerably from the corrected intensity functions of the AAAM and AAAA multilayers with diffraction maxima of lesser relative magnitudes at higher q_z and less-defined diffraction minima.

The Fourier transform of the corrected meridional intensity function yields the autocorrelation function of the multilayer electron density profile ([1]). Auto-

([1]) Strictly, electron density contrast due to truncation of $I(q_z)$ for $q_z \lesssim 0.01$ A^{-1}.

correlation functions for the AAAA, AAAM, and AAMM multilayers are shown in figure 2. These typical multilayer profile autocorrelation functions decay monotonically to essentially zero for $z > z_{max}$ which defines the extent of the multilayer profiles. z_{max} was found to be 96 Å, 108 Å, and 116 Å for the AAMM, AAAM, and AAAA multilayers respectively. The multilayer autocorrelation functions contain small amplitude low-frequency oscillations around the zero-baseline for $z > z_{max}$ due to errors ($\sim$ 2-5 %) in the corrected intensity functions for $q_z \leqslant \sim 0.02$ A^{-1}. These errors are a consequence of our background scattering correction.

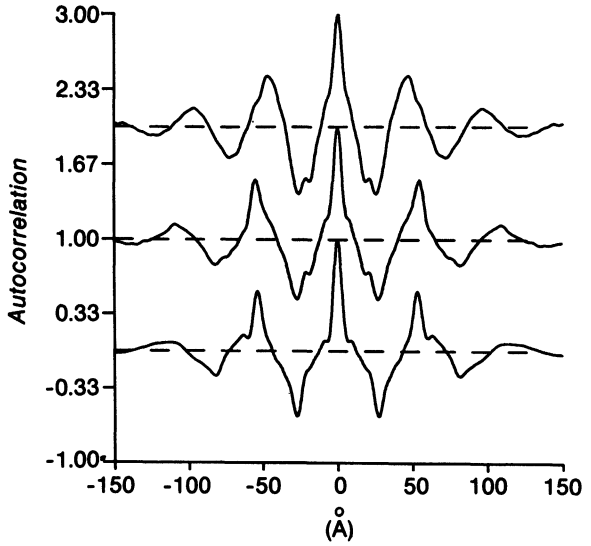

Fig. 2. — The Patterson functions for the AAMM (top), AAAM (middle), and AAAA (bottom) multilayers. Note the shift to larger absolute z of the positive correlation at $|z| \sim 110$ Å as the multilayer increases in overall size (top to bottom).

The multilayer autocorrelation functions for the DDDA and the DDD multilayers are shown in figure 4. The DDD multilayer was produced by washing the DDDA multilayer for three minutes in a 10 mM aqueous solution of NaOH [5]. The autocorrelation function calculated for the DDDA multilayer has pronounced positive correlations for $z \sim z_{max}$ ($\sim$ 110 A) while the autocorrelation function calculated for the DDD multilayer has only negative correlations for $z \sim z_{max}$ (90 A).

We have added an additional constraint to the iterative box-refinement technique [6] which is applicable when one wishes to determine the multilayer electron density profiles of several closely related multilayer thin films. Box refinement itself requires that the electron density profile of the multilayer being refined be of finite extent. The additional criterium that we have established for our enhanced refinement (or « corefinement ») requires that the multilayer thin films in question form a homologous series ; namely, we assume that the profile structures for these multilayers are the same over a specified region. Thus the AAAA, AAAM, and AAMM multilayers are assumed to form a homologous series with the first two monolayers in each of the multilayers being an identical arachidic acid bilayer.

The corefinement technique then adds the additional constraint to the box refinement procedure demanding that the two or more electron density profiles being simultaneously refined (i.e. corefined) refine to profiles with the same electron density over the assumed appropriate region in real space. This is accomplished by numerically averaging the resultant electron density profiles over this corefined region of real space after each iteration. Corefinement may then be allowed to relax its additional constraint after a specified number of iterations.

Figure 3 shows the multilayer electron density profiles for the AAAA multilayer corefined with the AAAM multilayer, the AAAA multilayer corefined with the AAMM multilayer, and the AAMM multilayer corefined with the AAAM multilayer. In each case the electron density profiles were corefined over the region 31 Å $< z <$ 150 Å; this region encompasses the first two arachidic acid monolayers. Relatively sharp, electron deficient troughs representing well-ordered terminal methyl groups are found at z = 84 Å and z = 32 Å, and an electron dense peak representing carboxyl headgroups is evident at z = 57 Å in each multilayer electron density profile. The last monolayer in each multilayer profile has a broad, electron deficient trough representing disordered terminal methyl groups at $z \sim -24$ Å for the AAAA multilayer, $z \sim -20$ Å for the AAAM multilayer, and $z \sim -11$ Å for the AAMM multilayer. The carboxyl head group peak region between the third and fourth monolayers is at z = 10 Å for the

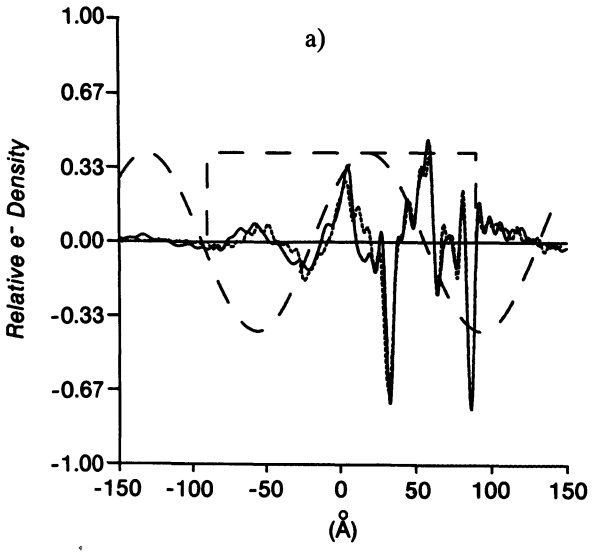

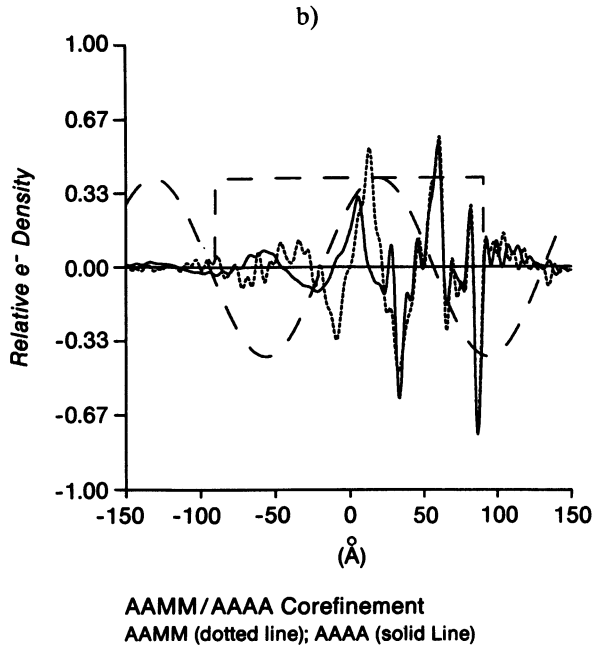

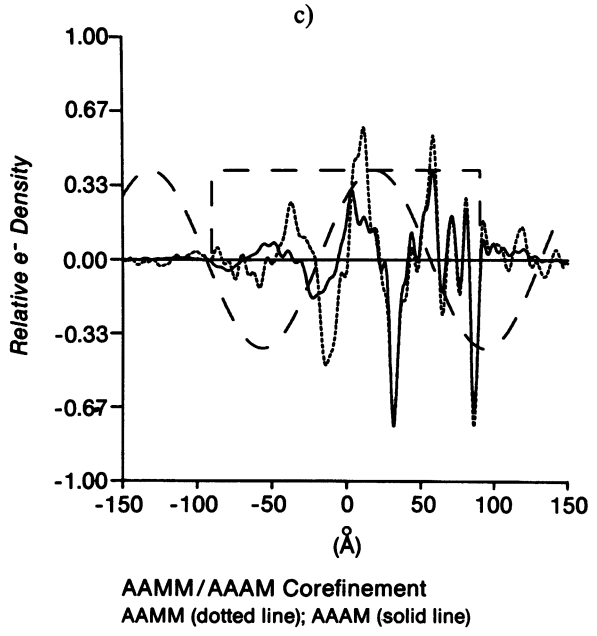

Fig. 3. — The electron density profiles derived by our variant of box refinement are shown. These profiles were corefined for five iterations and allowed to relax for an additional iteration. The refinements were corefined in real space for $z > 35$ Å. Figure 3a compares the electron density profiles derived by corefining the AAAA (solid line) and the AAAM (dotted line) multilayers. Figure 3b compares the electron density profiles derived by corefining the AAAA (solid line) and the AAMM (dotted line) multilayers. Figure 3c compares the electron density profiles derived by corefining the AAAM (solid line) and the AAMM (dotted line) multilayers. The initial trial function and the « box » used to truncate the profiles after each iteration are shown as dashed lines in each figure.

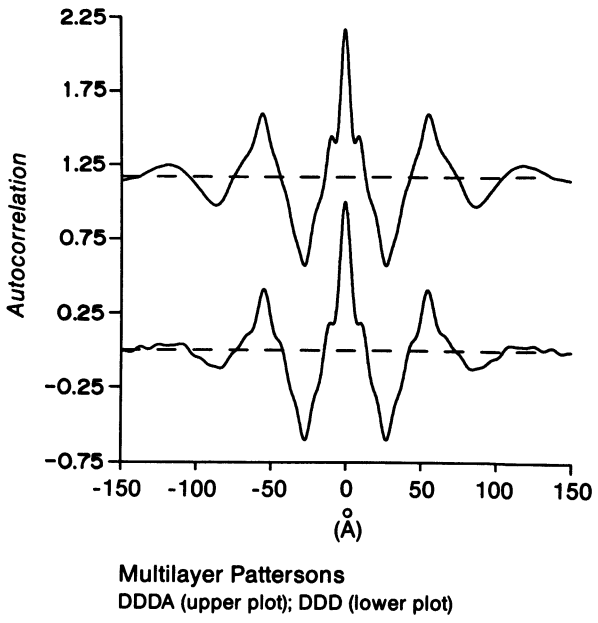

Fig. 4. — The Patterson functions for the DDDA (upper) and the DDD (lower) multilayers are compared. Note the disappearance of the positive correlation at $|z| \sim 110$ Å in the DDD Patterson function.

AAMM multilayer, and at $z = 2$ Å for the AAAM and AAAA multilayers.

Figure 5 shows the derived multilayer electron density profiles for the DDDA multilayer and the DDD multilayer. The two profiles (thin solid lines)

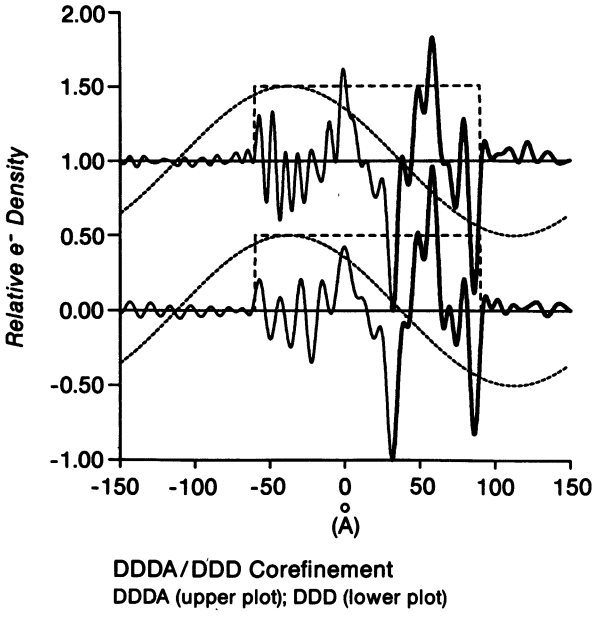

Fig. 5. — The derived electron density profiles for the DDDA (upper) and DDD (lower) multilayers are shown. The profiles were corefined for ten iterations and allowed to relax for one additional iteration. The heavy line represents to corefined region in the refinement. The trial function (dotted line) and the « box » (dashed line) used in truncating the profiles after each iteration are also shown.

were corefined using the same initial trial (dotted lines) and box functions (dashed lines), and allowed to iterate eleven times. The region in real space where the two profiles were constrained to have the same electron densities are shown by the heavy solid lines. Both multilayer electron density profiles have sharp troughs representing well-ordered terminal methyl groups at $z = 85$ Å and $z = 30$ Å, and a carboxyl headgroup peak at $z = 57$ Å. Two features in figure 5 should be noted. First, the carboxyl headgroup peak at $z \sim 0$ Å shows a significant decrease in electron density comparing the DDD multilayer electron density profile with the DDDA multilayer electron density profile. Second, the entire region -30 Å $\leqslant z \leqslant 0$ Å in the DDDA multilayer electron density profile, corresponding to the broad trough of disordered terminal methyl groups and adjacent hydrocarbon chain region of the arachidic acid monolayer, has a relative electron density well below zero level. For $z < -30$ Å the profile for the DDDA multilayer simply oscillates about zero electron density level. For the DDD multilayer, the electron density profile simply oscillates about the zero level for $z < -5$ Å.

4. Discussion.

The decreasing values of z_{max} for the multilayer profile autocorrelation functions for the AAAA, AAAM, and AAMM multilayers are consistent with the expected changes in the extent of the multilayer profiles. However, difficulty in determining z_{max} with certainty due to errors in $I\left(q_z < \sim 0.02\ \text{Å}^{-1}\right)$ limits its usefulness in the determination of the precise extent of the multilayer profiles (Fig. 2). Periodic multilayers, where the unit cell translation vector projected onto the z-axis has magnitude d, have autocorrelation functions which contain local maxima at integer multiples of d. In figure 2 the aucorrelation function of the AAAA multilayer shows such a local maximum at $|z| = 54$ Å dominated by the entirely positive correlations between the first monolayer and the third monolayer and between the second monolayer and the fourth monolayer ; in addition a local minimum occurs at $|z| = 27$ Å dominated by the negative correlations between the electron deficient terminal methyl groups $\left(-CH_3\right)$ of the arachidic acid monolayers and the electron dense carboxyl headgroups (—COOH) of adjacent monolayers. The autocorrelation function of the AAMM multilayer has a local maximum at $|z| \simeq 48$ Å with distinct shoulders at $|z| \simeq 54$ Å and $|z| \simeq 38$ Å; and local minima at $|z| \simeq 27$ Å and $|z| \simeq 19$ Å. Note the absence of such features at $|z| \simeq 19$ Å, $|z| \simeq 38$ Å, and $|z| \simeq 48$ Å in the autocorrelation function for the AAAA multilayer. In addition note the appearance of a positive shoulder at $|z| \simeq 48$ Å and a distinct negative feature at $|z| \simeq 19$ Å in the autocorrelation function for the AAAM multilayer. The derived electron density profiles for the AAAA, AAAM, and AAMM multilayers (Fig. 3) yield an average myristic acid carboxyl-methyl distance per monolayer of 22 ± 1 Å and an average arachidic acid carboxyl-methyl distance per monolayer of 27 ± 1 Å. The features noted above in the autocorrelation functions of the AAAA, AAAM, and AAMM multilayer profiles clearly demonstrate the sensitivity of the multilayer profile autocorrelation function in detecting changes in composition of the monolayers in the multilayer thin film.

The hydrocarbon chains of the macromolecules in one monolayer at the edge of each multilayer profile are significantly disordered as evidenced by a relatively broad methyl trough feature consistently at one end of the multilayer electron density profile. From the electron density profiles, the calculated difference in the average carboxyl-methyl end group distance between the arachidic acid and the myristic acid monolayers as noted above is consistently ~ 5 Å for the AAAA, AAAM, and AAMM multilayers. Hence, by varying the carboxyl-methyl end group distance for the last one or two monolayers in the deposition sequence by substituting myristic acid for arachidic acid in the AAAA/AAAM/AAMM experiments, we observed the appropriate shifting of the broad methyl trough feature at one end of the electron density profile (AAAA *versus* AAAM), or the appropriate shifting of both the broad methyl trough feature and the adjacent carboxyl headgroup region (AAAA *versus* AAMM, AAAM *versus* AAMM) in the multilayer electron density profiles (Fig. 3). The changes in the multilayer electron density profile of the DDDA multilayer (Fig. 5) upon the removal of the final arachidic acid monolayer to form the DDD multilayer is clearly evident. The electron density profile for the latter shows the absence of the broad methyl trough at $z = -25$ Å, as well as the decrease by factor of two of the carboxyl head group peak feature between the third and fourth monolayer at $z \simeq 0$ Å when the fourth monolayer is removed. The multilayer profile autocorrelation functions for the DDDA and DDD multilayers are consistent with the removal of the last arachidic acid monolayer. The pronounced positive correlations for $z \sim z_{max}$ $(\sim 110$ Å) for the DDDA multilayer are between the electron deficient terminal methyl group regions of the first (D) and last (A) monolayers deposited. The only negative correlations for $z \sim z_{max}$ $(\sim 90$ Å) for the DDD multilayer are between the electron dense carboxyl headgroup region of the last or third monolayer (D) and the electron deficient terminal methyl group region of the first monolayer (D) at the OTS-glass substrate surface. Therefore, since we know the sequence in which the different macromolecular monolayers were deposited during the fabrication of the multilayers, the two sets of experiments detailed in this communication unambiguously demonstrate that the surface monolayer at the multilayer-air interface is disordered. Conversely, the monolayer at the OTS-glass substrate surface, as well as all interior monolayers in the multilayer are well-ordered.

5. Conclusion.

In our previous work with the homologous series of multilayers AAAAAA, AAAA, and AA, we were unable to conclusively determine whether the first fatty acid monolayer (juxtaposed with the glass-OTS substrate) or the last surface monolayer (interfaced with air) in the monolayer deposition sequence was responsible for the broad methyl trough feature at one edge of the multilayer electron density profiles [3]. We simply demonstrated that on a macromolecular scale, one monolayer at one edge of the multilayer profile was consistently disordered ; all other monolayers in the multilayers containing one, two, three and five bilayers were well-ordered. By systematically varying the chain length of the fatty acid molecules in the different monolayers of the multilayer, we were able to prove that the last or surface monolayer in the deposition sequence was indeed the disordered monolayer. In addition, when we chemically removed the last deposited monolayer, the multilayer electron density profile no longer exhibited the broad methyl trough feature at one end. Since the multilayer films were non-periodic, standard structural methods which rely on the repetition of an average structural unit could not be employed. However, the box refinement technique is a very powerful method for solving the phase problem in structures which are of finite extent. Unfortunately, box refinement alone generally cannot provide a unique phase solution which satisfies the box refinement constraint of zero electron density contrast outside the box for asymmetric structures [7]. Usually some additional criteria must also be used. Applying the box refinement techniques to series of homologous multilayers allows one to confidently establish the correct electron density profile. The corefinement technique employed is effectively the real space analog of holographic interferometry described previously [8]. It utilizes the reasonable physical-chemical constraint that the multilayer structures in the homologous series remain invariant over a specified region in real space.

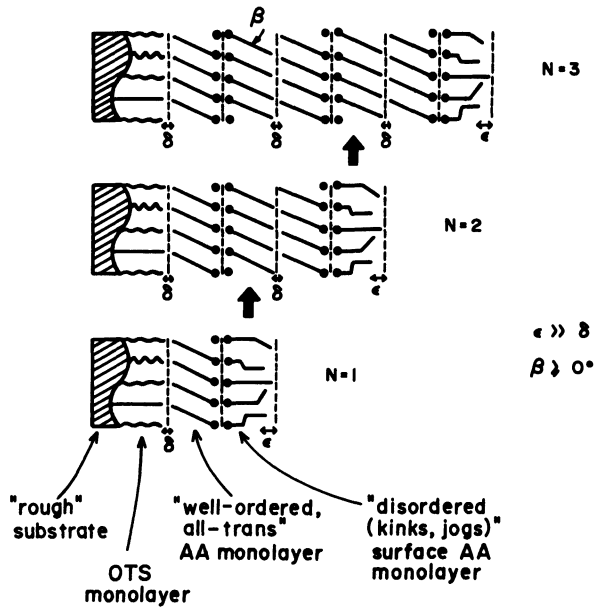

Fig. 6. — The figure contains a schematic representation of our current knowledge concerning the structure of ultrathin multilayer films of *arachidic acid* (AA) deposited via the Langmuir-Blodgett technique on *alkylated glass substrates* as derived from our analyses of high-resolution (Δq_z) X-ray scattering data along q_z. The glass substrate is depicted as being « rough » on the length-scale of the alkylating C_{18} chains of OTS. However, the terminal methyl group ends of the OTS chains are depicted to all lie within a thin layer of width δ parallel to the substrate plane also containing the apposed terminal methyl groups of the adjacent overlayer of arachidic acid ; this result is based on the width and relative depth of the sharp trough at the substrate-end of the multilayer electron density profile (3) and the very small mosaic spread of these ultrathin multilayers (3) for $N = 1$, 2, 3 and 5. Hence, the C_{18} chains of the OTS appear to smooth out the « roughness » of the glass substrate *in the presence of* an overlayer of arachidic acid *via* variable C_{18} chain configurations. With the exception of the arachidic acid monolayer at the multilayer-air interface, all interior arachidic acid monolayers in the multilayer are depicted as being well-ordered, composed virtually exclusively of all-trans chain configurations with the chain axis oriented at an angle β relative to the perpendicular to the layer plane ; this result is based on the widths δ and relative amplitudes of the terminal methyl group features and similarly the carboxyl polar headgroup features in the multilayer electron density profiles and on the so-derived carboxyl-methyl endgroup distance (*) in the multilayer profile projection (3). The arachidic acid monolayer at the multilayer-air interface is depicted as being disordered *via* chain configurations containing « kinks » and « jogs » which disorder the terminal methyl groups over ε along the multilayer profile axis ; this result is based on the broad electron deficient feature which always occurs at the air-end of the multilayer electron density profile (3) when the multilayer surface is composed of non-polar terminal methyl groups (as opposed to carboxyl polar headgroups). The heavy vertical arrows indicate the overlayer induced ordering phenomenon which occurs upon deposition of an additional monolayer(s).

(*) The measured average carboxyl-methyl endgroup distance (27 ± 1 Å) for the interior monolayers is sufficient to allow well-ordered, all-trans arachidic acid chains to be perpendicular to the layer plane. However, given the finite spatial resolution of the derived multilayer electron density profiles, the all-trans chains could also be significantly tilted relative to the layer plane depending on the exact geometry of the carboxyl-carboxyl interaction between the apposed monolayers. In fact, the measured carboxyl-methyl endgroup distances appear to vary systematically from 28 Å to 26 Å depending on the monolayer's position in the multilayer profile suggesting a corresponding systematic variation in β [9]. We note that chain tilt relative to the layer plane can also be measured independently (on the *same* specimens under *identical* conditions) *via* X-ray scattering parallel to the layer planes requiring synchrotron radiation for such ultrathin multilayer films *and* that such chain tilt may depend upon the degree of ionization of the carboxyl group.

Our previous work coupled with our current results necessarily leads us to conclude that the surface monolayer of an amphiphilic molecule at the multilayer-air interface in Langmuir-Blodgett multilayer thin films can be ordered by the deposition of another bilayer (or monolayer). These results are summarized in figure 6. This overlayer-induced ordering of the underlying monolayer is not only interesting in statistical mechanical terms concerning relevant physical interactions between the different monolayers in the multilayer, but it must also be considered in the fabrication of stable Langmuir-Blodgett multilayer films where intramolecular/intermolecular ordering within a monolayer is critical for device applications.

Acknowledgments.

This work was supported by the NIH grant GM 33525, the NSF program grant DMR 8216718, and the AFOSR grant 84-0135.

References

[1] GARITO, A. F., SINGER, K. D. and TENG, C. C., in *Nonlinear Optical Properties of Organic and Polymer Materials,* D. Williams, editor (ACS Symp. Ser. No.) **223** (1983).

[2] GARITO, A. F. and SINGER, K. D., *Laser Focus* **18** (1982) 59.

[3] SKITA, V., FILIPKOWSKI, M., GARITO, A. and BLASIE, J. K., *Phys. Rev.* **B** (in press).

[4] SAGIV, J., *JACS* **102** (1980) 92.

[5] MCLEAN, L. R., AZIZ, D. A., WHITTAM, M. A., JOHNSTON, D. S. and CHAPMAN, D., *Thin Solid Films* **99** (1983) 127.

[6] STROUD, R. M. and AGARD, D. A., *Biophys. J.* **25** (1979) 495.

[7] MAKOWSKI, L., *J. Appl. Cryst.* **14** (1981) 160.

[8] LESSLAUER, W. and BLASIE, J. K., *Acta Cryst.* **A 27** (1971) 456.

[9] FISCHETTI, R., FILIPKOWSKI, M., GARITO, A., and BLASIE, J. K., (manuscript in preparation).